



Numerical simulation of laminar plasma dynamos in a cylindrical von Kármán flow

I. V. Khalzov, B. P. Brown, F. Ebrahimi, D. D. Schnack, and C. B. Forest

Citation: *Phys. Plasmas* **18**, 032110 (2011); doi: 10.1063/1.3559472

View online: <http://dx.doi.org/10.1063/1.3559472>

View Table of Contents: <http://pop.aip.org/resource/1/PHPAEN/v18/i3>

Published by the [American Institute of Physics](#).

Additional information on Phys. Plasmas

Journal Homepage: <http://pop.aip.org/>

Journal Information: http://pop.aip.org/about/about_the_journal

Top downloads: http://pop.aip.org/features/most_downloaded

Information for Authors: <http://pop.aip.org/authors>

ADVERTISEMENT

The advertisement features a green and white wavy background. At the top, the 'AIP Advances' logo is shown with a series of orange dots forming an arc above the word 'Advances'. Below this, the text 'Special Topic Section: PHYSICS OF CANCER' is written in white on a dark green background. At the bottom, the phrase 'Why cancer? Why physics?' is written in white, followed by a blue button with the text 'View Articles Now' in white.

AIP Advances

Special Topic Section:
PHYSICS OF CANCER

Why cancer? Why physics? [View Articles Now](#)

Numerical simulation of laminar plasma dynamos in a cylindrical von Kármán flow

I. V. Khalzov,¹ B. P. Brown,¹ F. Ebrahimi,² D. D. Schnack,¹ and C. B. Forest¹

¹University of Wisconsin, 1150 University Avenue, Madison, Wisconsin 53706, USA

²University of New Hampshire, 8 College Road, Durham, New Hampshire 03824, USA

(Received 4 December 2010; accepted 2 February 2011; published online 24 March 2011)

The results of a numerical study of the magnetic dynamo effect in cylindrical von Kármán plasma flow are presented with parameters relevant to the Madison Plasma Couette Experiment. This experiment is designed to investigate a broad class of phenomena in flowing plasmas. In a plasma, the magnetic Prandtl number Pm can be of order unity (i.e., the fluid Reynolds number Re is comparable to the magnetic Reynolds number Rm). This is in contrast to liquid metal experiments, where Pm is small (so, $Re \gg Rm$) and the flows are always turbulent. We explore dynamo action through simulations using the extended magnetohydrodynamic NIMROD code for an isothermal and compressible plasma model. We also study two-fluid effects in simulations by including the Hall term in Ohm's law. We find that the counter-rotating von Kármán flow results in sustained dynamo action and the self-generation of magnetic field when the magnetic Reynolds number exceeds a critical value. For the plasma parameters of the experiment, this field saturates at an amplitude corresponding to a new stable equilibrium (a laminar dynamo). We show that compressibility in the plasma results in an increase of the critical magnetic Reynolds number, while inclusion of the Hall term in Ohm's law changes the amplitude of the saturated dynamo field but not the critical value for the onset of dynamo action. © 2011 American Institute of Physics. [doi:10.1063/1.3559472]

I. INTRODUCTION

The dynamo phenomenon, where magnetic fields are self-generated by a moving and electrically conducting fluid, is one of the most intriguing subjects of modern magnetohydrodynamics (MHD). Dynamos have particularly important applications in astrophysics.^{1,2} Today, it is widely believed that the magnetic fields of planets and stars originate from dynamo action in their interiors.^{3–5} As far as we know, all astrophysical dynamos are turbulent with extremely high fluid Reynolds numbers, Re , which makes theoretical treatments very involved and realistic simulations are currently impossible. At the same time, some key physical processes likely at work in astrophysical dynamos can be revealed by considering idealized laminar dynamos related to spatially smooth stationary velocity fields at comparatively low Re . In particular, the theoretical study of laminar dynamos allows one to determine the critical magnetic Reynolds number above which dynamo excitation takes place to find the structure and magnitude of a saturated dynamo field and to understand the influence on the dynamo of different plasma effects, such as compressibility, two-fluid effects, and anisotropic transport.

A number of laminar MHD flows appropriate for dynamo generation have been analyzed in the literature.^{6–11} In most of these studies, only the kinematic dynamo problem has been considered, in which the magnetic induction equation is solved as an eigenvalue problem for a given velocity field (not necessarily satisfying the Navier–Stokes equation) to find the growth rate of the magnetic field. The nonlinear feedback of the fields on the flows is ignored in the kinematic treatment. Among the laminar flows that lead to kinematic dynamos at sufficiently high magnetic Reynolds num-

bers are cylindrical helical jets (Ponomarenko dynamo⁶), two-dimensional spatially periodic arrays of helical jets (Roberts' scheme⁷), cylindrical von Kármán⁸ and Taylor–Couette flows,⁹ and spherical Dudley–James flows.¹⁰ The first three of these flows have been tested recently in experiments with liquid sodium, and successful observations of dynamo action have been reported in Refs. 12–14. The flows in these experiments were turbulent, thus making it difficult to compare experimental data with predictions of laminar dynamo theory, although in the first two, the role of turbulence was small as the flows were strongly constrained. This is a common disadvantage of all liquid metal dynamo experiments: the extremely low magnetic Prandtl numbers (the ratio of kinetic viscosity ν to resistivity η or, equivalently, the ratio of magnetic Reynolds to fluid Reynolds $Pm = \nu / \eta = Rm / Re \sim 10^{-5}$ for liquid sodium) requires very high fluid Reynolds numbers ($Re \sim 10^6–10^7$) in order to achieve the magnetic Reynolds number sufficient for dynamo action ($Rm \sim 10^1–10^2$) in liquid metals. As a result, the relevant flow is always turbulent.

The present paper is motivated by the Madison Plasma Couette Experiment (MPCX),¹⁵ which is designed to study MHD phenomena driven by plasma flows. One of the novelties of this experiment is the ability to change the magnetic Prandtl number of the plasma by several orders of magnitude from $Pm \ll 1$ to $Pm \gg 1$. This flexibility makes it possible to investigate laminar dynamos by choosing a regime with $Pm \sim 1–10$ and $Re \sim 10^2$. As a result, the direct comparison of experimental data with numerical simulations of laminar dynamo can be performed. Such a comparison can also be used for the first time to test different MHD models as well as the numerical codes which simulate them.

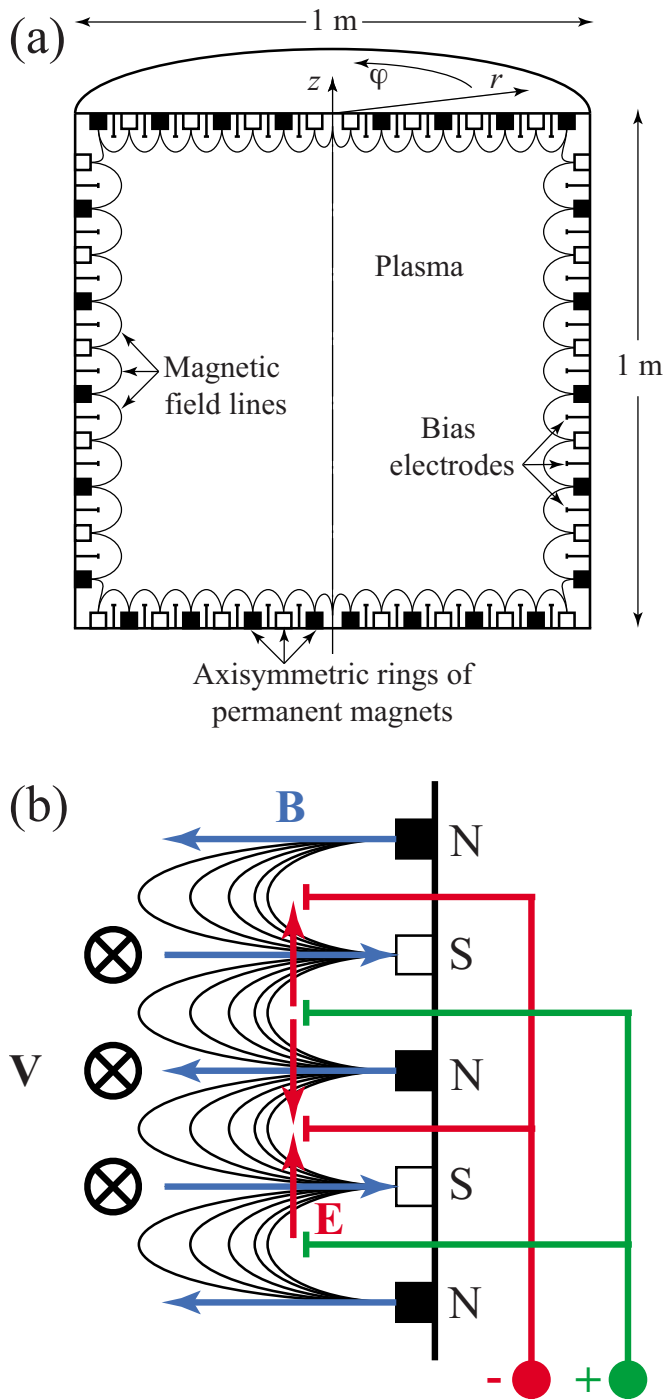


FIG. 1. (Color online) Madison Plasma Couette Experiment (MPCX): (a) sketch; (b) partial vertical cross section. Rings of permanent magnets of alternating polarity line the inside of the cylinder with their poles oriented normally to the walls. Ring anodes and cathodes are placed between the magnets. The resulting $\mathbf{E} \times \mathbf{B}$ drift is in the azimuthal direction. By varying the potential between the anodes and cathodes, the velocity forcing at the outer boundary can be customized.

The goal of this study is to investigate possible dynamo action in the MPCX using the extended MHD code NIMROD,¹⁶ which can accurately model plasma dynamics in the specific geometry for realistic experimental conditions. Among the features of NIMROD is the possibility to study effects beyond standard MHD, including the addition of the Hall term in Ohm's law. The effect of the Hall term on dy-

namo action has recently been studied in periodic box simulations,^{17,18} and the Hall term will almost certainly play an important role in the MPCX. The results of our simulations can also be used for the optimization of plasma parameters and as guidance for the experimental operation.

In this paper, we report the results of NIMROD simulations of a laminar magnetic dynamo in the cylindrical von Kármán flow under conditions relevant to the MPCX. Simulations are done for an isothermal compressible MHD plasma model with and without two-fluid effects (the Hall term). The structure of the paper is as follows. In Sec. II, we briefly review the MPCX experiment and describe the NIMROD plasma model. In Sec. III, the hydrodynamical properties of von Kármán flow are studied. In Sec. IV, the kinematic dynamo problem is considered for von Kármán flow in a cylinder, and the self-generation of the magnetic field is demonstrated for parameters achievable in the experiment. In Sec. V, the results of simulations of nonlinear dynamo saturation are presented, and the effect of the Hall term is studied. In Sec. VI, we conclude with a discussion of the effects that can influence the magnetic dynamo in such plasma flows.

II. NIMROD MODELS OF MPCX

The MPCX is closely related to the spherical plasma experiment described in Ref. 19, though here the geometry is cylindrical and the apparatus is somewhat smaller in size (1 m in diameter). In the MPCX, the plasma is confined by a multicusp magnetic field created by axisymmetric rings of permanent magnets of alternating polarity and localized at the boundary of the cylindrical chamber (Fig. 1). There are 10 magnetic rings at the cylindrical wall and 8 at both the top and bottom end-caps. Ring anodes and cathodes positioned between the magnet rings can be biased with arbitrary potentials. The resulting $\mathbf{E} \times \mathbf{B}$ drift of plasma is in the azimuthal direction and can be an arbitrary axisymmetric function at the boundary of the vessel. This arrangement allows arbitrary shear flows to be imposed in the MPCX.

The use of a plasma gives experimentalists great flexibility in choosing the regimes of operation. By varying the plasma density (gas flow rate), ion mass (H, He, Ne, Ar), electron temperature (heating power), and flow speed (bias potentials of electrodes), a wide range of parameters can be achieved in experiment (Table I). Such flexibility is advantageous over the liquid metal dynamo experiments, where Pm is fixed and small. For a description of the plasma parameters in our simulations, we introduce several standard dimensionless numbers: magnetic Prandtl

$$Pm \equiv \frac{\nu}{\eta} = 46 \frac{T_e^{3/2}[\text{eV}] T_i^{5/2}[\text{eV}]}{n_0 [10^{18} \text{ m}^{-3}] \mu_i^{1/2} \lambda^2}, \quad (1)$$

fluid Reynolds

$$Re \equiv \frac{R_0 V_0}{\nu} = 0.52 \frac{R_0 [\text{m}] V_0 [\text{km/s}] n_0 [10^{18} \text{ m}^{-3}] \mu_i^{1/2} \lambda}{T_i^{5/2} [\text{eV}]}, \quad (2)$$

TABLE I. Parameters of MPCX.

Quantity	Symbol	Value	Unit
Radius of cylinder	R_0	0.5	m
Height of cylinder	H	1	m
Peak driving velocity	V_0	0–20	km/s
Average number density	n_0	10^{17} – 10^{19}	m^{-3}
Electron temperature	T_e	2–10	eV
Ion temperature	T_i	0.5–4	eV
Ion species		H, He, Ne, Ar	
Ion mass	μ_i	1, 4, 20, 40	amu
Ion charge	Z	1	e
Magnetic Prandtl	Pm	1×10^{-3} – 5×10^2	
Fluid Reynolds	Re	0 – 4×10^4	
Magnetic Reynolds	Rm	0 – 1×10^3	
Mach	M	0–4	
Hall	ε	0.15–1.8	

magnetic Reynolds

$$Rm \equiv \frac{R_0 V_0}{\eta} = 24 \frac{R_0[\text{m}] V_0[\text{km/s}] T_e^{3/2}[\text{eV}]}{\lambda}, \quad (3)$$

Mach

$$M \equiv \frac{V_0}{C_s} = 0.10 \frac{V_0[\text{km/s}] \mu_i^{1/2}}{\gamma^{1/2} T_e^{1/2}[\text{eV}]}, \quad (4)$$

Hall

$$\varepsilon \equiv \frac{c}{R_0 \omega_{pi}} = 0.23 \frac{\mu_i^{1/2}}{R_0[\text{m}] n_0^{1/2} [10^{18} \text{ m}^{-3}]}, \quad (5)$$

where ν is the plasma kinematic viscosity, η is the magnetic diffusivity, λ is the Coulomb logarithm (typically $\lambda \approx 10$ – 20), C_s is the ion sound speed, γ is the adiabatic index, c is the speed of light, ω_{pi} is the ion plasma frequency, and other parameters are defined in Table I. Equations (1)–(3) for numerical estimates of Pm , Re , and Rm are derived from Braginskii equations for a plasma with singly charged ions in a weak magnetic field;²⁰ the weak-field approximation is reasonable for the bulk of MPCX because the high-multipole cusp field is concentrated mostly near the wall and quickly falls off away from it. The typical values of these nondimensional numbers are listed in Table I. For convenience, we also give the “inverse” mapping formulary: peak driving velocity, km/s

$$V_0 = 2.54 \frac{\lambda^{1/4} \gamma^{3/8} Rm^{1/4} M^{3/4}}{\mu_i^{3/8} R_0^{1/4}[\text{m}]}, \quad (6)$$

average number density, 10^{18} m^{-3}

$$n_0 = 0.053 \frac{\mu_i}{\varepsilon^2 R_0^2[\text{m}]}, \quad (7)$$

electron temperature, eV

$$T_e = 0.065 \frac{\lambda^{1/2} \mu_i^{1/4} Rm^{1/2}}{\gamma^{1/4} M^{1/2} R_0^{1/2}[\text{m}]}, \quad (8)$$

ion temperature, eV

$$T_i = 0.35 \frac{\lambda^{1/2} \mu_i^{9/20} \gamma^{3/20} Rm^{1/10} M^{3/10}}{\varepsilon^{4/5} Re^{2/5} R_0^{1/2}[\text{m}]}. \quad (9)$$

The results presented in this paper are obtained using the extended MHD code NIMROD.¹⁶ As a simulation framework, we choose the isothermal Hall MHD approach. This is one of the simplest NIMROD models allowing for two-fluid effects and compressibility, and this appears to be a good approximation for the plasma under experimental conditions. The equations of this model in nondimensional form are

$$\frac{\partial n}{\partial \tau} = -\nabla \cdot (n\mathbf{v}), \quad (10)$$

$$\begin{aligned} n \frac{\partial \mathbf{v}}{\partial \tau} = & -n(\mathbf{v} \cdot \nabla)\mathbf{v} - \frac{1}{M^2} \nabla n + (\nabla \times \mathbf{b}) \times \mathbf{b} \\ & + \frac{1}{Re} \left(\nabla^2 \mathbf{v} + \frac{1}{3} \nabla (\nabla \cdot \mathbf{v}) \right), \end{aligned} \quad (11)$$

$$\frac{\partial \mathbf{b}}{\partial \tau} = \nabla \times \left(\mathbf{v} \times \mathbf{b} - \frac{\varepsilon}{n} (\nabla \times \mathbf{b}) \times \mathbf{b} \right) + \frac{1}{Rm} \nabla^2 \mathbf{b}. \quad (12)$$

In these equations, τ , n , \mathbf{v} , and \mathbf{b} stand for normalized time, number density, velocity, and magnetic field, respectively:

$$\tau = \frac{V_0 t}{R_0}, \quad n = \frac{\rho}{n_0 m_i}, \quad \mathbf{v} = \frac{\mathbf{V}}{V_0}, \quad \mathbf{b} = \frac{\mathbf{B}}{V_0 \sqrt{4\pi n_0 m_i}},$$

where ρ is the mass density and m_i is the ion mass. The unit of length is the cylinder radius R_0 , while V_0 is the peak velocity of the driven von Kármán flow. An important difference of this system of Eqs. (10)–(12) from a standard single-fluid MHD model is the inclusion of the Hall term in the magnetic induction Eq. (12), which takes into account two-fluid effects. The magnitude of this term is characterized by the nondimensional Hall number ε . We will consider simulations where the Hall term is significant ($0 < \varepsilon < 1$) and others where it is absent ($\varepsilon = 0$). The simulations are performed in a nonrotating cylindrical coordinate system (r, φ, z) , with the plasma occupying the region $(0 < r < 1, -1 < z < 1)$.

The Hall MHD Eqs. (10)–(12) also require the specification of boundary conditions. Two different sets of boundary conditions are used in the simulations. Set I is used only to demonstrate the possibility of stirring the plasma with the applied multicusp magnetic field and an appropriately modulated tangential electric field at the boundary. In set I, no-slip, stationary, and rigid walls are assumed, so all components of the velocity vanish at the boundary,

$$\mathbf{v}|_{\Gamma} = 0. \quad (13)$$

For the magnetic and electric fields in set I, we assume perfectly conducting walls, implying that the time-varying normal component of the magnetic field and the time-varying tangential component of the electric field are zero at the boundary,

$$\tilde{b}_n|_{\Gamma} = 0, \quad \tilde{E}_t|_{\Gamma} = 0, \quad (14)$$

where the normalized electric field is

$$\mathbf{E} = -\mathbf{v} \times \mathbf{b} + \frac{\varepsilon}{n}(\nabla \times \mathbf{b}) \times \mathbf{b} + \frac{1}{Rm} \nabla \times \mathbf{b}.$$

Note that the externally applied time-independent multicusp magnetic field \mathbf{b}_0 and boundary electric field \mathbf{E}_0 do not satisfy Eq. (14), and thus provide $\mathbf{E}_0 \times \mathbf{b}_0$ stirring at the boundary. Using different modulations of the tangential boundary electric field, we have successfully simulated several types of flows. Figure 2 shows the results for the so-called von Kármán flow, in which plasma is driven in opposite azimuthal directions near the top and bottom end-caps. Having demonstrated that $\mathbf{E}_0 \times \mathbf{b}_0$ stirring will successfully drive a von Kármán flow under realistic experimental conditions, we now turn to a simpler set of boundary conditions.

All results reported in the later sections are obtained with the boundary conditions of set II. In set II, we ignore the applied multicusp magnetic field and the tangential electric field. Instead, we assume that the driving of the plasma is due to differentially rotating walls. This assumption greatly simplifies the model and allows us to focus on the physics of the dynamo action and not on details of the plasma driving. The boundary conditions for the full electric and magnetic fields are

$$b_n|_{\Gamma} = 0, \quad E_t|_{\Gamma} = 0 \quad (15)$$

(perfectly conducting walls), and the velocity conditions are

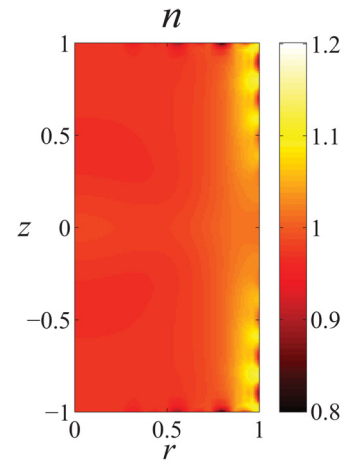
$$\begin{aligned} \mathbf{v}|_{r=1} &= z\mathbf{e}_{\varphi}, \\ \mathbf{v}|_{z=-1} &= -r\mathbf{e}_{\varphi}, \end{aligned} \quad (16)$$

$$\mathbf{v}|_{z=1} = r\mathbf{e}_{\varphi}$$

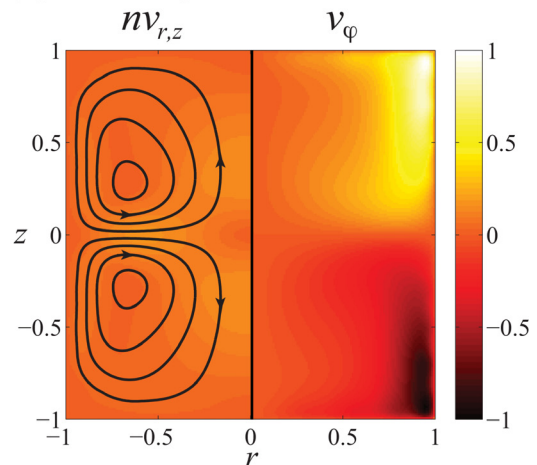
(no-slip differentially rotating rigid walls). These velocity boundary conditions correspond approximately to von Kármán flow: the top and bottom end-caps are counter-rotating with the same angular velocity, and the side wall has a linear dependence of angular velocity on z to match the rotation of top and bottom end-caps. This flow is the primary object of our dynamo study.

We briefly remark on the spatial and temporal resolution used in these simulations. For spatial discretization, NIMROD employs a high order finite element method in r - and z -directions and a pseudospectral method in periodic φ -direction with dependence $e^{im\varphi}$ for each Fourier harmonic (integer m represents the azimuthal mode number). The basis functions of the finite elements are polynomials. In all of the simulations presented here, we have used a uniform meshing of the r - z plane with 8×16 finite elements each of polynomial degree 3, and 11 Fourier harmonics in the azimuthal φ -direction. This spatial resolution appears to be sufficient for the laminar flows under consideration. To verify the simulation results obtained at this resolution, we have repeated a nonlinear MHD run introduced in Sec. V using mesh with 16×32 finite elements in r - z plane and 11 azimuthal modes. The time dynamics of the flow and the mag-

(a) Number density



(b) Velocity



(c) Magnetic field

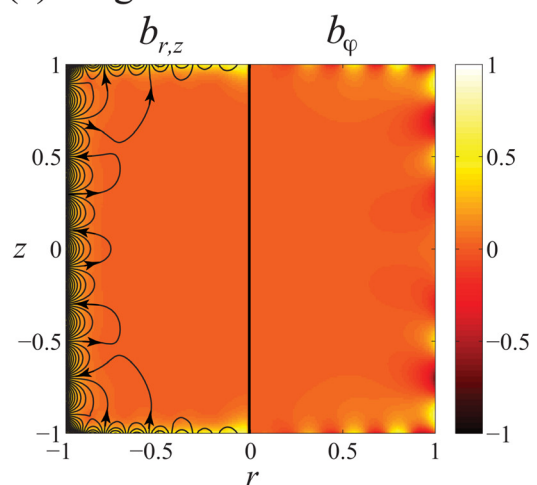


FIG. 2. (Color online) Structure of axisymmetric equilibrium von Kármán flow driven by electromagnetic system at the boundary for Mach number $M=1$, fluid Reynolds number $Re=200$, and magnetic Reynolds number $Rm=20$: (a) number density; (b) velocity; (c) magnetic field. Cross-sections in r - z plane are given. Left panels of (b) and (c) show stream lines of poloidal parts (r - and z -components) of flux $n\mathbf{v}$ and magnetic field \mathbf{b} , respectively, superimposed on absolute values of these parts depicted in colors. Right panels of (b) and (c) show azimuthal components of corresponding fields.

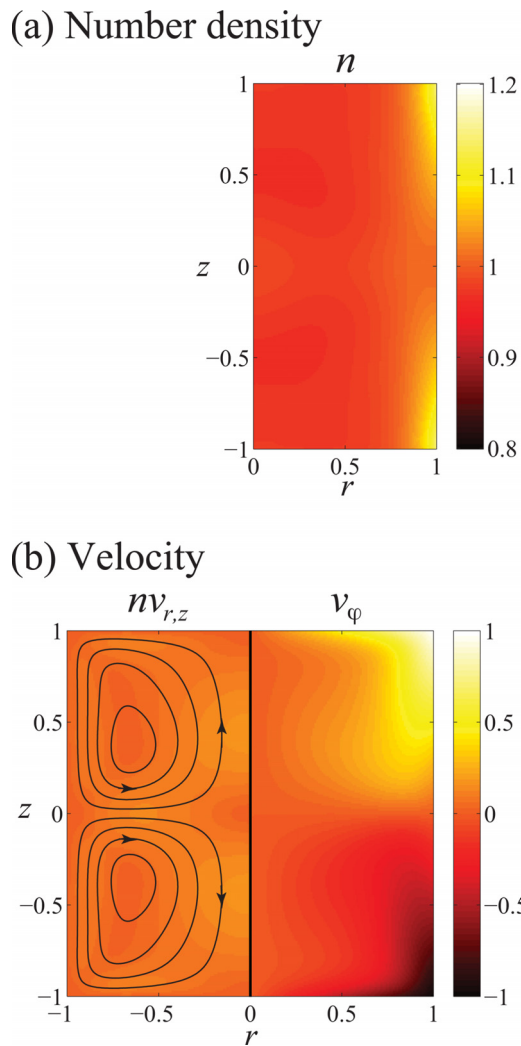


FIG. 3. (Color online) Structure of axisymmetric equilibrium von Kármán flow driven by differentially rotating walls for Mach number $M=1$ and fluid Reynolds number $Re=200$: (a) number density; (b) velocity. The same elements as in Fig. 2 are shown.

netic field were fully reproduced, which confirms that a converged solution is obtained already at the coarser resolution. The solutions are time-evolved using a semi-implicit staggered leap-frogging algorithm, which is fully detailed in Refs. 16 and 21. We should emphasize here that the algorithm employed in NIMROD can be made numerically stable for arbitrarily large time-steps in both single-fluid and Hall MHD by choosing the appropriate coefficients of the semi-implicit operators.²¹ However, in order to accurately model the temporal behavior of the system with significant flows, in the present simulations we have used an adaptive time-step based on the explicit Courant–Friedrichs–Lewy (CFL) condition for advection. Even in the dynamo simulations, we find that advection by the axisymmetric velocity field dominates the CFL criteria, rather than either the Alfvén or whistler waves associated with the relatively weak magnetic fields.

III. HYDRODYNAMICAL EQUILIBRIUM AND STABILITY

In this section, we consider the basic hydrodynamical (no magnetic field, $\mathbf{b}=0$) properties of von Kármán flow in a cylinder, in which the plasma is stirred at the edge via the

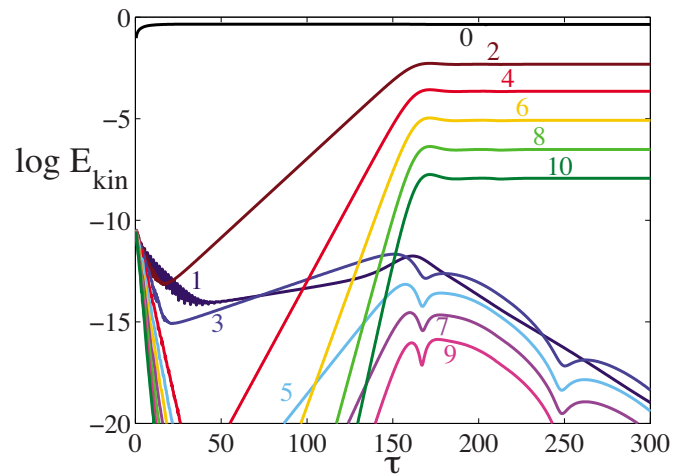


FIG. 4. (Color online) Time dynamics of kinetic energy of different azimuthal harmonics in purely hydrodynamical ($\mathbf{b}=0$) von Kármán flow for Mach number $M=1$ and fluid Reynolds number $Re=200$. Corresponding azimuthal mode numbers m are shown.

boundary conditions of set II [Eq. (16)]. We start with the axisymmetric case, assuming that physical quantities do not depend on φ , i.e., $\partial/\partial\varphi=0$. The axisymmetric equilibrium flow structure for fluid Reynolds number $Re=200$ and Mach number $M=1$ is shown in Fig. 3. The velocity components are either symmetric (radial v_r) or antisymmetric (azimuthal v_φ and axial v_z) with respect to equatorial plane $z=0$, and the azimuthal velocity has maxima at the corners of the cylinder. The flow develops two cells of poloidal (in the r - z plane) circulation with inward direction at the equatorial plane. Such flow pattern leads to the stratification of density, which builds up near the corners of the cylinder.

The axisymmetric equilibrium von Kármán flow becomes unstable with respect to nonaxisymmetric perturbations when the fluid Reynolds exceeds a critical value (Fig. 4). This instability is the Kelvin–Helmholtz type instability, occurring due to the presence of unstable velocity shear in the fluid. For Mach number $M=1$, the critical value of the Reynolds number is about $Re \approx 160$. As shown in Fig. 4, within approximately one viscous time, the unstable modes grow and saturate at a new equilibrium state, which consists of the axisymmetric part and relatively small nonaxisymmetric distortions with even azimuthal mode numbers, $m=2, 4, 6, \dots$. Such a transition to nonaxisymmetric equilibrium is crucial for the dynamos considered here.

The structure of the equilibrium von Kármán flow, in particular the amplitude of the nonaxisymmetric distortions, depends on the Reynolds and Mach numbers (Fig. 5). As we discuss in Sec. IV, such dependence affects the critical value of the magnetic Reynolds number above which the dynamo is excited.

IV. KINEMATIC DYNAMO

Our first step in this dynamo study is to solve the kinematic dynamo problem: determining the possibility of self-generation of magnetic field for a given flow structure. For fixed fluid Reynolds and Mach numbers, we solve the stationary time-independent ($\partial/\partial\tau=0$) continuity [Eq. (10)] and

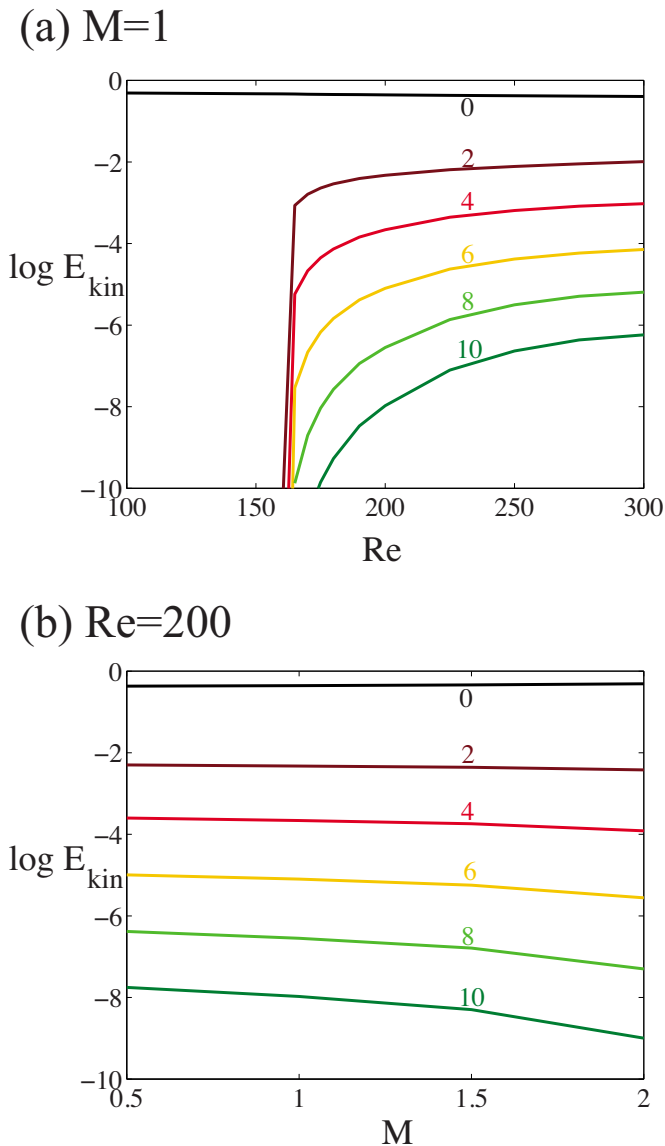


FIG. 5. (Color online) Kinetic energy of different azimuthal harmonics in hydrodynamically stable von Kármán flow as a function of (a) fluid Reynolds number Re for Mach number $M=1$; (b) Mach number M for fluid Reynolds number $Re=200$. Corresponding azimuthal mode numbers m are shown.

Navier–Stokes [Eq. (11)] equations and find the steady-state hydrodynamic equilibrium velocity \mathbf{v}_{eq} (which includes possible nonaxisymmetric distortions). Using that velocity, we solve induction Eq. (12) as an eigenvalue problem for a magnetic field with different magnetic Reynolds numbers

$$\gamma \mathbf{b} = \nabla \times (\mathbf{v}_{\text{eq}} \times \mathbf{b}) + \frac{1}{Rm} \nabla^2 \mathbf{b}, \quad (17)$$

where γ is an eigenvalue. This allows us to determine the critical magnetic Reynolds above which the dynamo excitation is possible. The results are presented in Fig. 6. The dependence of the critical magnetic Reynolds on the fluid Reynolds for Mach number $M=1$ is shown in Fig. 6(a). The vertical line at $Re \approx 160$ separates the regions of axisymmetric ($Re < 160$) and nonaxisymmetric ($Re > 160$) von Kármán flows. Our simulations show that the kinematic dynamos are

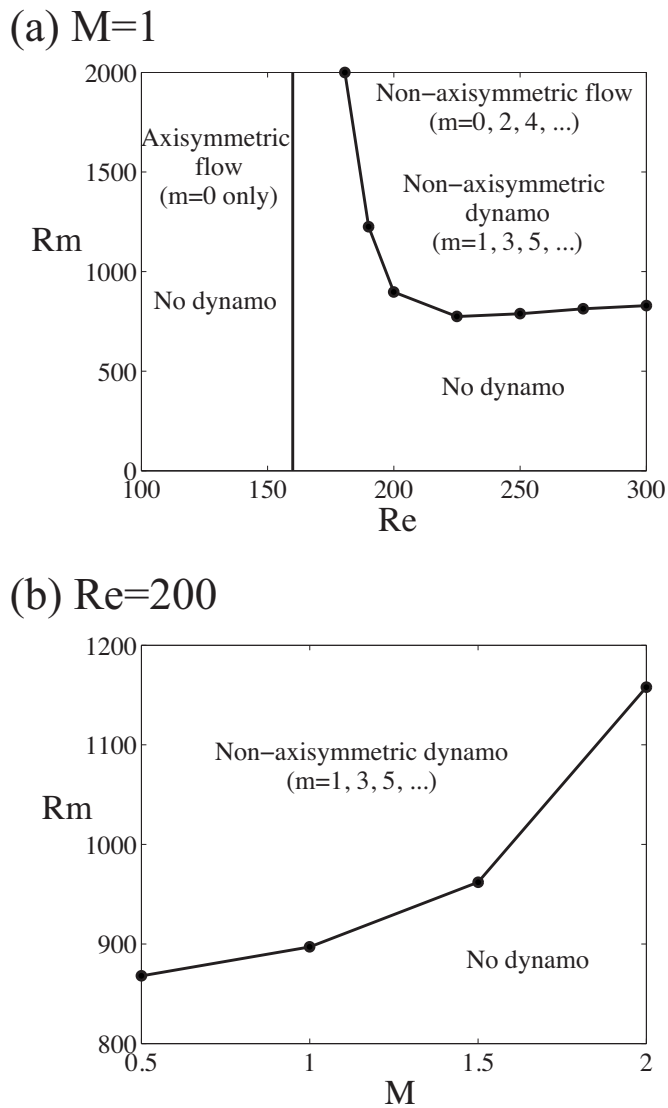


FIG. 6. Critical magnetic Reynolds number Rm as a function of (a) fluid Reynolds number Re for Mach number $M=1$; (b) Mach number M for fluid Reynolds number $Re=200$. Vertical line in (a) separates the regions of axisymmetric and nonaxisymmetric equilibrium von Kármán flows.

not possible in axisymmetric flows. In nonaxisymmetric flow at sufficiently high magnetic Reynolds number Rm , the dynamo appears as a growing magnetic field with odd azimuthal harmonics, $m=1, 3, 5, \dots$

In our study of the plasma dynamo, we use a compressible fluid model. Compressibility is related to the Mach number [Eq. (4)]—the ratio of the peak driving velocity to the sound speed. In general, the higher Mach number, the more compressible the fluid, i.e., the more stratified its density. An increase in the Mach number leads to changes in the equilibrium velocity field \mathbf{v}_{eq} and, in particular, decreases the energy in the nonaxisymmetric components of the flow [Fig. 5(b)]. This, in turn, affects the kinematic dynamo problem [Eq. (17)] by increasing the value of the critical Rm [Fig. 6(b)].

From a comparison of Figs. 5 and 6, we can conclude that the dynamo action in the case under consideration is related to the nonaxisymmetric part of the von Kármán flow: the stronger the nonaxisymmetric distortions, the lower the

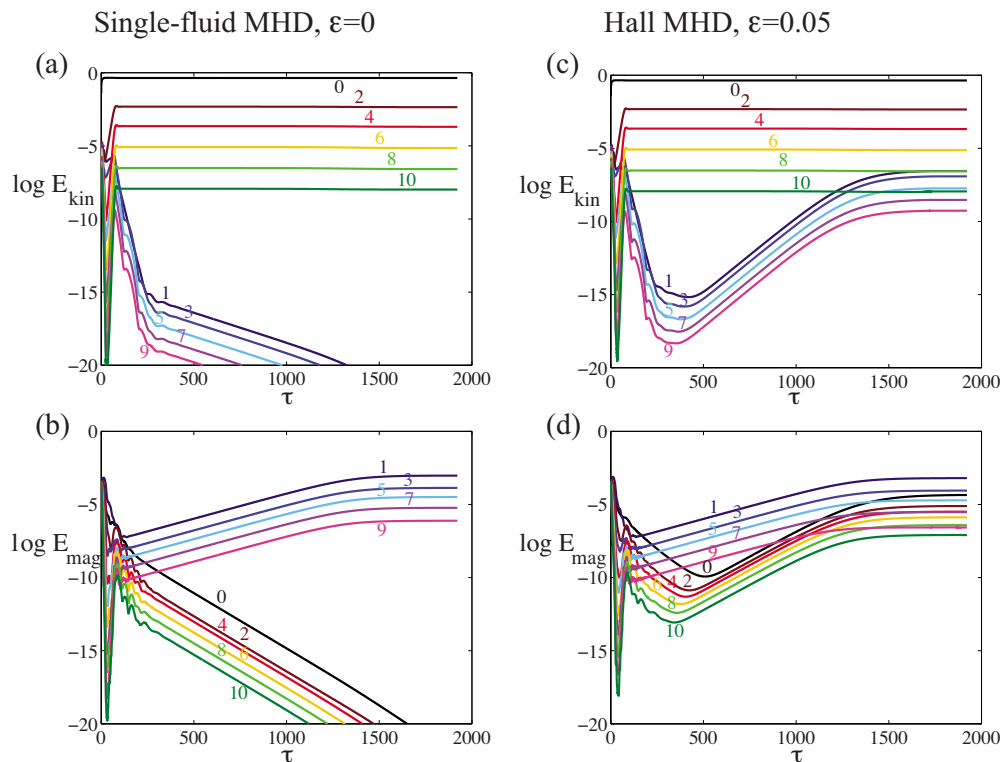


FIG. 7. (Color online) Time dynamics of kinetic E_{kin} and magnetic E_{mag} energies of different azimuthal modes in von Kármán flow for Mach number $M=1$, fluid Reynolds $Re=200$, and magnetic Reynolds $Rm=1000$, with azimuthal mode numbers m labeled. [(a),(b)] Single-fluid MHD case ($\epsilon=0$). Flows are of even m modes while fields are odd in m . [(c),(d)] Hall MHD case ($\epsilon=0.05$). Initial behavior is similar to the single-fluid MHD case, but as the fields become strong ($\tau \approx 500$), the Hall effect becomes important. The final equilibrium includes both odd and even m .

threshold value of magnetic Reynolds number for the onset of the dynamo.

V. NONLINEAR SATURATION OF DYNAMO FIELD

Next, we analyze the state of the fully saturated dynamo generated magnetic field and its back reaction on the flow. In this section, we report the results of fully nonlinear simulations of the system [Eqs. (10)–(12)]. The nondimensional parameters are chosen to be $Re=200$, $Rm=1000$, $M=1$, and $\epsilon=0.05$ – 1.0 (for Hall MHD runs); simulations with these parameters achieve fully saturated laminar states for the dynamo fields and the fluid flows.

Figures 7(a) and 7(b) demonstrate the time dynamics of the kinetic and magnetic energies for a single-fluid MHD case ($\epsilon=0$). After the initial transient phase ($\tau \approx 100$), the flow becomes stationary. It is primarily axisymmetric, with nonaxisymmetric distortion consisting of even azimuthal harmonics ($m=2, 4, 6, \dots$) and containing only about 1% of the total kinetic energy. In such a flow, the dynamo is excited: the magnetic field of odd harmonics ($m=1, 3, 5, \dots$) grows exponentially in time until it saturates at $\tau \approx 1500$. In some sense, the saturated magnetic field is in equipartition with the nonaxisymmetric part of the flow. Here, E_{mag} is about 0.3% of the total energy of the flow E_{kin} . Due to the lack of an axisymmetric magnetic field ($m=0$) and the small amplitude of the nonaxisymmetric fields, the back reaction of the

dynamo magnetic field on the axisymmetric flow is very weak and the imposed von Kármán flow is essentially unmodified. The structure of the saturated magnetic field, with the $m=1$ azimuthal harmonic visibly dominating the overall structure, is shown in Fig. 8(a).

In the Hall MHD case ($\epsilon=0.05$), the dynamics of the system is different [Figs. 7(c) and 7(d)]. After the nonaxisymmetric flow with even modes develops (at $\tau \approx 100$), the odd harmonics of the magnetic field start to grow, as in a single-fluid MHD case. Now, however, when the odd harmonics of the magnetic field become large enough (at $\tau \approx 500$), the Hall effect becomes significant and other harmonics of the flow and the magnetic field grow, breaking the initial even-odd symmetry. The saturated state of the flow and the magnetic field contains all harmonics, though the dominating parts are similar to a MHD case. The structure of the saturated Hall dynamo field for $\epsilon=0.5$ is shown in Fig. 8(b).

Figure 9 shows the dependence of the magnetic energy for different azimuthal modes in the saturated state on the Hall number ϵ . It is worth noting that the presence of the Hall effect not only breaks the even-odd symmetry of the system, but also reduces the energy of the saturated dynamo field. For $\epsilon \geq 0.2$ the energy of the saturated dynamo field scales as $E_{\text{mag}} \propto \epsilon^{-2}$ ($b \propto \epsilon^{-1}$ for the field amplitude). This is a direct consequence of the magnetic induction Eq. (12), which in a saturated state ($\partial/\partial\tau=0$) now reads

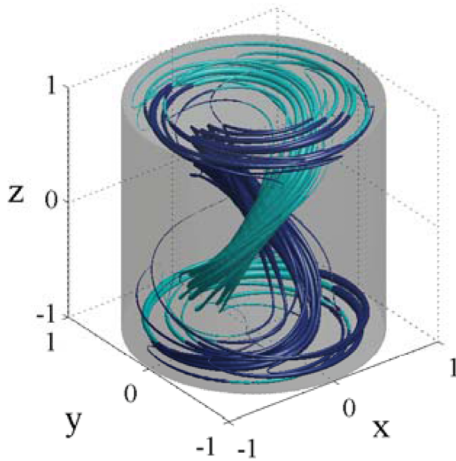
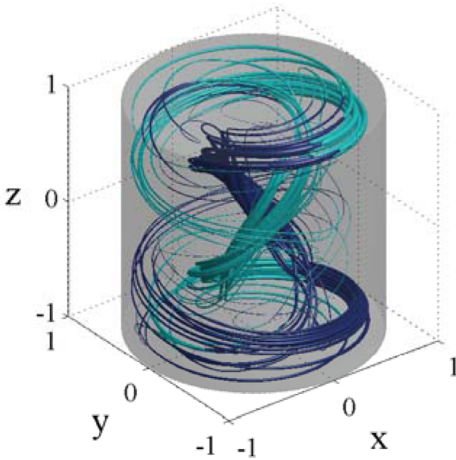
(a) Single-fluid MHD dynamo, $\varepsilon=0$ (b) Hall MHD dynamo, $\varepsilon=0.5$ 

FIG. 8. (Color online) Magnetic field lines of saturated dynamos: (a) single-fluid MHD case ($\varepsilon=0$); (b) Hall MHD case ($\varepsilon=0.5$). Thickness of the line is proportional to the magnitude of the field, while lighter (darker) color corresponds to upward (downward) direction of the field.

$$\nabla \times \left(\mathbf{v} \times \mathbf{b} - \frac{\varepsilon}{n} (\nabla \times \mathbf{b}) \times \mathbf{b} \right) + \frac{1}{Rm} \nabla^2 \mathbf{b} = 0. \quad (18)$$

Indeed, if the magnetic Reynolds number Rm and functions \mathbf{v} and n are independent of ε , then the solution for the magnetic field \mathbf{b} can be written as

$$\mathbf{b} = \frac{\mathbf{h}}{\varepsilon}, \quad (19)$$

where \mathbf{h} is a vector-function independent of ε satisfying equation

$$\nabla \times \left[\mathbf{v} \times \mathbf{h} - \frac{1}{n} (\nabla \times \mathbf{h}) \times \mathbf{h} \right] + \frac{1}{Rm} \nabla^2 \mathbf{h} = 0 \quad (20)$$

and boundary conditions [Eq. (15)]. In the case under consideration, it is clear that the scaling used in Eq. (19) is valid only asymptotically for large Hall numbers ε when the mag-

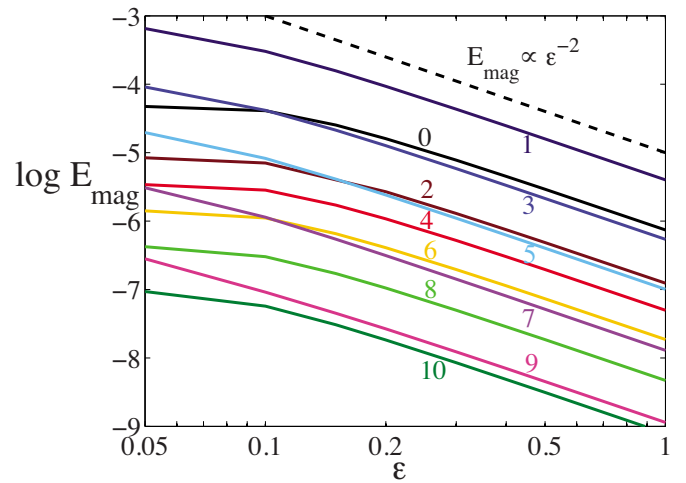


FIG. 9. (Color online) Magnetic energy of different azimuthal harmonics in saturated Hall MHD dynamo as a function of the Hall number ε . Azimuthal mode numbers m are shown. Dashed line corresponds to scaling $E_{\text{mag}} \propto \varepsilon^{-2}$.

netic field \mathbf{b} is small and its influence on the flow is negligible. Under these assumptions, the plasma velocity \mathbf{v} and density n do not depend on ε and correspond to the purely hydrodynamical equilibrium that is determined by the fluid Reynolds Re and Mach M numbers (as described in Sec. III). Thus, for relatively large Hall parameters ($\varepsilon \geq 0.2$), the saturation of the dynamo takes place due to the back reaction of the Hall term in induction Eq. (12) long before the amplitude of the magnetic field is large enough to change the flow significantly. This is in contrast to the single-fluid MHD dynamo (and the Hall dynamo with $\varepsilon \ll 0.1$), where the saturated state is achieved due to modification of the flow profile by the growing dynamo field before the Hall effect plays a considerable role. Scaling [Eq. (19)] suggests that the Hall effect is unfavorable for the dynamo.

We note Refs. 22–24, where results of simulations for a single-fluid MHD dynamo in a sphere with counter-rotating incompressible flows are reported. Despite the difference in geometry, our MHD results are in qualitative agreement with the cases of laminar dynamos from Refs. 22 and 23, which have dominant $m=0$ and $m=2$ harmonics in kinetic energy and $m=1$ harmonic in magnetic energy during the saturation phase. However, in contrast to the results of Ref. 24, we do not observe the generation of an axial magnetic dipole with $m=0$ and quasiperiodic oscillations.

VI. DISCUSSION

We have performed numerical simulations of a plasma dynamo for cylindrical von Kármán flow using the extended MHD code NIMROD. These NIMROD simulations provide numerical support for the Madison Plasma Couette Experiment (MPCX). We have demonstrated that sustained dynamo action and self-generation of magnetic field can be attained for parameters that are achievable in the experiment. Our results show that the critical magnetic Reynolds number required for dynamo excitation strongly depends on the plasma compressibility: the more compressible the fluid, the higher the critical Rm (Fig. 6). Inclusion of two-fluid effects into the

model (in the form of the Hall term in the induction equation) does not influence the critical Rm , but does change the structure of the saturated flow and the dynamo field (Fig. 7). The effect of the Hall term on dynamo field is negative: the energy of the saturated magnetic field scales as $1/\varepsilon^2$ when the Hall number is $\varepsilon \gtrsim 0.2$ (Fig. 9).

The simulations show that the presence of nonaxisymmetric distortions in the flow plays a decisive role in dynamo excitation. Such distortions with even azimuthal mode numbers ($m=2,4,6,\dots$) appear in the flow only for modest values of fluid Reynolds number $Re > 160$ when the axisymmetric shear flow becomes hydrodynamically unstable. Therefore, in order to observe the dynamo effect in the MPCX, the plasma has to be driven above a critical hydrodynamical threshold. For a helium plasma with number density $n_0=10^{18} \text{ m}^{-3}$, electron temperature $T_e=16 \text{ eV}$, and ion temperature $T_i=0.9 \text{ eV}$, the peak driving velocity should be $V_0=20 \text{ km/s}$.

Another issue is related to the detection of the laminar dynamo field in the experiment. Since the saturated magnetic energy of the dynamo field is only a small fraction of the total kinetic energy, the resulting dynamo field is relatively weak. For the helium plasma considered above, the volume-averaged saturated dynamo magnetic field is $B_0 \approx 0.1 \text{ G}$. Such a small field is still detectable even on the background of the much stronger multicusp field from the rings of magnets (about 10^3 G near the walls) due to the different azimuthal symmetries of these two fields.

Lastly, we remark on the model used in our simulations. The single-fluid MHD model ($\varepsilon=0$) is adequate for predicting critical magnetic Reynolds numbers and the thresholds for sustained dynamo action. The fully nonlinear saturated dynamo state differs, however, when the Hall effect is included. It appears that the isothermal Hall MHD model ($\varepsilon>0$) is a good “rough” approximation for the plasma under experimental conditions, but this model also does not capture the full details of the plasma dynamics. Other effects such as thermal conductivity, electron pressure, and anisotropic viscosity can all play important roles in a real plasma experiment. These effects will be the subject of future studies.

ACKNOWLEDGMENTS

The authors wish to thank Dr. C. Sovinec for valuable help and discussions related to NIMROD. The work is supported by the National Science Foundation.

- ¹H. K. Moffatt, *Magnetic Field Generation in Electrically Conducting Fluids* (Cambridge University Press, Cambridge, 1978).
- ²A. Brandenburg and K. Subramanian, *Phys. Rep.* **417**, 1 (2005).
- ³M. Ossendrijver, *Astron. Astrophys. Rev.* **11**, 287 (2003).
- ⁴P. Charbonneau, *Living Rev. in Solar Phys.* **7**, 3 (2010).
- ⁵C. A. Jones, *Annu. Rev. Fluid Mech.* **43**, 583 (2010).
- ⁶Yu. B. Ponomarenko, *J. Appl. Mech. Tech. Phys.* **14**, 775 (1975).
- ⁷G. O. Roberts, *Philos. Trans. R. Soc. London, Ser. A* **271**, 411 (1972).
- ⁸L. Marié, J. Burguete, F. Daviaud, and J. Léorat, *Eur. Phys. J. B* **33**, 469 (2003).
- ⁹P. Laure, P. Chossat, and F. Daviaud, *NATO Science Series II: Math., Phys., Chem.* **26**, 17 (2000).
- ¹⁰M. L. Dudley and R. W. James, *Proc. R. Soc. London, Ser. A* **425**, 407 (1989).
- ¹¹D. Moss, *Geophys. Astrophys. Fluid Dyn.* **102**, 195 (2008).
- ¹²A. Gailitis, O. Lielausis, S. Dement'ev, E. Platacis, A. Cifersons, G. Gerbeth, T. Gundrum, F. Stefani, M. Christen, H. Hänel, and G. Will, *Phys. Rev. Lett.* **84**, 4365 (2000).
- ¹³R. Stieglitz and U. Müller, *Phys. Fluids* **13**, 561 (2001).
- ¹⁴R. Monchaux, M. Berhanu, M. Bourgoïn, M. Moulin, Ph. Odier, J.-F. Pinton, R. Volk, S. Fauve, N. Mordant, F. Pétrélis, A. Chiffaudel, F. Daviaud, B. Dubrulle, C. Gasquet, L. Marié, and F. Ravelet, *Phys. Rev. Lett.* **98**, 044502 (2007).
- ¹⁵C. Collins, C. B. Forest, R. Kendrick, and J. Jara-Almonte, *Bull. Am. Phys. Soc.* **53**, 298 (2008).
- ¹⁶C. R. Sovinec, A. H. Glasser, T. A. Gianakon, D. C. Barnes, R. A. Nebel, S. E. Kruger, D. D. Schnack, S. J. Plimpton, A. Tarditi, M. S. Chu, and NIMROD Team, *J. Comput. Phys.* **195**, 355 (2004).
- ¹⁷P. D. Mininni, D. O. Gómez, and S. M. Mahajan, *Astrophys. J.* **587**, 472 (2003).
- ¹⁸D. O. Gómez, P. D. Mininni, and P. Dmitruk, *Phys. Rev. E* **82**, 036406 (2010).
- ¹⁹E. J. Spence, K. Reuter, and C. B. Forest, *Astrophys. J.* **700**, 470 (2009).
- ²⁰S. I. Braginskii, *Reviews of Plasma Physics* (Consultants Bureau, New York, 1965), Vol. 1, p. 205.
- ²¹C. R. Sovinec, J. R. King, and NIMROD Team, *J. Comput. Phys.* **229**, 5803 (2010).
- ²²R. A. Bayliss, C. B. Forest, M. D. Nornberg, E. J. Spence, and P. W. Terry, *Phys. Rev. E* **75**, 026303 (2007).
- ²³K. Reuter, F. Jenko, A. Tilgner, and C. B. Forest, *Phys. Rev. E* **80**, 056304 (2009).
- ²⁴C. Gissinger, E. Dormy, and S. Fauve, *Phys. Rev. Lett.* **101**, 144502 (2008).